Current Research in Microbial Sciences 9 (2025) 100428

Contents lists available at ScienceDirect

Current Research in Microbial Sciences

journal homepage: www.sciencedirect.com/journal/current-research-in-microbial-sciences

Intratumor *Rhodococcus* sp. *B513* drives DEN-induced hepatocellular carcinoma progression by modulating gut microbiota and angiogenesis

Qisha Liu [a,b,1,*], Jingjing Wang [a,c,1], Yutong Yao [a], Xuqi Sun [d], Weijia Fang [d], Yewei Zhang [e], Zhi Liu [a,*], Yi Zheng [d,*]

[a] Key Laboratory of Pathogen of Jiangsu Province, Department of Pathogen Biology-Microbiology Division, Nanjing Medical University, Nanjing 211166, China
[b] National Demonstration Center for Experimental Basic Medical Education, Nanjing Medical University, Nanjing 211166, China
[c] The Affiliated Suzhou Hospital of Nanjing Medical University, Suzhou Municipal Hospital, Gusu School, Nanjing Medical University, Suzhou 215026, China
[d] Department of Medical Oncology, The First Affiliated Hospital, Zhejiang University School of Medicine, Hangzhou 310003, China
[e] Department of General Surgery, Second Affiliated Hospital of Nanjing Medical University, Nanjing 211166, China

ARTICLE INFO

Keywords:
Hepatocellular carcinoma
Rhodococcus
Vascular endothelial growth factor
Gut microbiota

ABSTRACT

Hepatocellular carcinoma (HCC) is the fourth leading cause of cancer-related mortality worldwide with challenging clinical treatment. Accumulating evidence demonstrates that gut dysbiosis promotes HCC progression, and intratumoral bacteria play an essential role in carcinogenesis by modulating the tumor immune microenvironment. However, the microbiome within liver tumor tissues remains poorly characterized. In this study, we investigated the intratumoral microbiota of HCC and identified a specific bacterial taxon, *Rhodococcus* sp. *B513*, that was enriched in tumor tissues. We found that *Rhodococcus* sp. *B513* promoted HCC development partially by inducing vascular endothelial growth factor (VEGF) expression and promoting angiogenesis. Moreover, *Rhodococcus* sp. *B513* induced gut dysbiosis in HCC model, characterized by an increased abundance of pro-inflammatory bacteria and a reduction in short-chain fatty acids (SCFA) producing bacteria. Furthermore, administration of *Rhodococcus* sp. *B513* introduced intestinal inflammation and permeability. Our results provided evidences for the cross-talk between the *Rhodococcus* sp. *B513* and HCC progression, and suggested the potential prognostic and therapeutic value of the *Rhodococcus* sp. *B513*.

1. Introduction

Liver cancer ranks as the fourth leading cause of cancer-related deaths globally (Singal et al., 2020). Our previous studies have indicated that modification of specific gut microbiota may provide therapeutic benefits for HCC patients (Liu et al., 2019). Currently, the diagnosis of HCC primarily relies on imaging or histopathological findings. Therefore, it is urgent to develop novel therapeutic targets for early prediction or diagnosis of HCC.

Recently, increasing studies have unraveled the existence of a distinct intratumoral microbiome that promotes tumorigenesis by modifying immune microenvironment and resistance against chemotherapy (Nejman et al., 2020; Dohlman et al., 2022). Considering that the liver is anatomically connected to the intestines via the portal vein, gut bacteria might be able to translocate to the liver in leaky gut states (Manfredo Vieira et al., 2018; Wang et al., 2025). For instance, *Stenotrophomonas maltophilia* was enriched in tumor tissues of HCC patients with cirrhosis, facilitating HCC progression by activating TLR-4-mediated NF-κB signalling pathway and secreting various inflammatory factors (Liu et al., 2022). Additionally, intratumoral *Paraburkholderia fungorum* could inhibit tumor growth through alanine, aspartate, and glutamate metabolism in intrahepatic cholangiocarcinoma (Chai et al., 2023). Despite these findings, intratumoral bacteria that mediate HCC progression remain largely unknown.

Here, we aimed to assess the intratumoral microbiome of HCC patients and to identify tumor-associated bacteria. *Rhodococcus* sp. *B513* was found to be enriched in hepatic tumor tissues. We further investigated the role of *Rhodococcus* sp. *B513* in the HCC progression and intestinal inflammation in mouse model. Our findings suggested that intratumor *Rhodococcus* sp. *B513* plays an important role in promoting HCC, intervention of which might therefore be worth exploring for advancing oncology care.

* Corresponding authors.
E-mail addresses: liuqisha@njmu.edu.cn (Q. Liu), liuzhi@njmu.edu.cn (Z. Liu), oncologist@zju.edu.cn (Y. Zheng).
[1] These authors contributed equally: Qisha Liu, Jingjing Wang.

https://doi.org/10.1016/j.crmicr.2025.100428

Available online 24 June 2025

2. Materials and methods

2.1. Clinical samples

We initially enrolled 8 HCC patients who underwent hepatectomy at the First Affiliated Hospital of Zhejiang University, and an additional validation cohort (10 HCC patients) were enrolled for validation. The exclusion criteria were as follows: (1) had received immunotherapy, radiotherapy, or chemotherapy prior to the hepatectomy, (2) HBsAg, HCVAb, diabetes, autoimmune disease, hypertension, inflammatory bowel diseases, HIV, any other types of liver diseases, (3) get antiviral therapy, alcohol abuse or antibiotics treatment in the past 6 months. The liver normal, peritumoral, and tumor tissues were collected under sterile condition. All fresh samples were immediately frozen with liquid nitrogen, and stored at -80 °C until used. All participants were provided a written informed consent upon enrolment. The steps were carried out in accordance with the Ethics Committee of the First Affiliated Hospital of Zhejiang University (permit #2020–343) and Ethics Committee of Nanjing Medical University (permit #2019–800).

2.2. Cell lines

The murine hepatocellular carcinoma H22, murine macrophage RAW264.7, human hepatocellular carcinoma HepG-2, and human umbilical vein endothelial cells (HUVEC) were obtained from the Second Affiliated Hospital of Nanjing Medical University. The cells were maintained in Dulbecco's modified Eagle's medium (DMEM) supplemented with 10 % fetal bovine serum (FBS) at 37 °C with 5 % CO_2 except for HUVECs. HUVECs were cultured in Endothelial Cell Medium (ECM) supplemented with 10 % FBS and 1 % endothelial cell growth supplement (ECGS; ScienCell, USA).

2.3. Bacterial culture and growth condition

In order to isolate bacteria from liver tissues, about 100 mg tissues were placed in 200 μL of 1 × PBS which containing glass beads. Samples were homogenized using a muti-tissue sample crusher (Shanghai Jingxin Industrial Developmental Company, China) for 60 s, then spin down at 3000 rpm for 30 s. The supernatants were inoculated on trypticase soy agar (TSA) culture medium, and incubated at 37 °C for 2–3 days. Genomic DNA extraction and 16S rRNA amplification were carried out from each clone. The 16S rRNA universal primers 27F (5′-AGAGTTTGATCCTGGCTCAG-3′) and 1492R (5′-GGTTACCTTGTTACGACTT-3′) were used for PCR amplication. The obtained sequences were compared through BLAST in NCBI. In addition, the specific primers Rho-F1 (5′-GTATCGCAGCCCTCTGTACC-3′) and Rho-R1 (5′-GCAGTAACTGACGCTGAGGA-3′) were used to amplify 16S rRNA fragment of *Rhodococcus* sp. *B513* with PCR amplication, resulting in fragments of 500 bps for identifying *Rhodococcus* sp. *B513*. *Rhodococcus* sp. *B513* were routinely grown in TSA or trypticase soy broth (TSB) medium at 37 °C for 48 h. The bacteria were stored at -80 °C until used. The 16S rRNA sequences of *Rhodococcus* sp. *B513* were submitted to NCBI with accession number OQ423203.

2.4. Phylogenetic analysis of Rhodococcus

To identify the genetic relationship of *Rhodococcus* sp. *B513* with other *Rhodococcus* species, the 16S rRNA sequences of 39 validated *Rhodococcus* species were obtained from GenBank. The phylogenetic tree was assessed by 1000 bootstrap using the MEGA software which computed by the neighbour- joining (NJ) analysis and maximum composite likelihood model, *Escherichia coli* sample was used as outgroup.

2.5. Antibiotic susceptibility testing

Minimum inhibitory concentration (MIC) were determined using a modified broth microdilution assays as previously described (Wiegand et al., 2008). Briefly, *Rhodococcus* sp. *B513* inoculated into 96-well microplate containing serially-diluted antibacterial agents: chloramphenicol, erythromycin, gentamicin, rifampicin, ampicillin, streptomycin, kanamycin, streptomycin, vancomycin, and tetracycline antibiotics (varied concentrations: 0.10, 0.20, 0.39, 0.78, 1.56, 3.13, 6.25, 12.5, 25, 50, 100, 200, and 400 μg/mL). Bacteria were cultured in TSB medium at 37 °C for 24 h. Experiments were carried out in three biological replicates.

2.6. Rhodococcus labelling with FDAA probes and macrophage infection

Rhodococcus sp. *B513* was labelled by fluorescent d-amino acid (FDAA; TADA-amide, 0.5 mM) according to the previously recorded (Wang et al., 2019; Lin et al., 2020). Bacteria were incubated in TSB supplemented with FDAA probes overnight at 37 °C. Labelled bacteria were then pelleted and washed twice with PBS, then resuspended in 200 μL PBS for infecting RAW264.7 cells. Cells were seeded on glass coverslips in 12-well dishes at 2×10^5 cells/well. The cells were exposed to FDAA-labelled *Rhodococcus* sp. *B513* for 30 min at 37 °C. Extracellular bacteria were washed by PBS containing 500 μg/mL gentamicin three times, followed by incubation in complete DMEM medium for 4 h. This concentration gentamicin inhibited the growth of extracellular bacteria without infiltrating eukaryotic plasma membranes (Wang et al., 2018). Then cells were fixed in 4 % paraformaldehyde for 10 min, and washed three times with PBS. Coverslips were mounted on glass slides using Antifade Mounting Medium with DAPI (Cat#P0131, Beyotime, China). Images were obtained using Zeiss LSM 800 Confocal Laser Scanning Microscopy under 40 × objective. FDAA probes were purchased from Chinese Peptide Company (Hangzhou, China).

2.7. Preparation of freeze-dried bacterial supernatant powder

Cell-free supernatant (CFS) powders of *Rhodococcus* sp. *B513* were prepared as previously described (Dimitrieva-Moats and Ünlü, 2012). Briefly, overnight cultures of bacteria were inoculated in 5-mL TSB medium to reach mid- or late exponential growth phase (A600 of 1.5–3.5). Cells were pelleted by centrifugation (15,000 g, 15 min at 4 °C), then added to 50-mL TSB and incubated for 24 h at 37 °C. The resulting fermentations were centrifuged (15,000 g, 15 min at 4 °C). *Rhodococcus* CFS powders were prepared by filter sterilization using 0.22-μm-pore-size filters and freeze-drying for 48 h using a Labconco FreeZone System. TSB freeze-dried powder was used as a control, which obtained using the same procedure. Powders were kept at -80 °C until further use. The powders were dissolved with sterile PBS at the same amount TSB before the cells are treated.

2.8. Transwell migration and invasion assay

The migration and invasion assays were performed using Transwell chambers (24-well insert, Corning, USA) as previously described (Liu et al., 2018). For migration assay, the 4×10^4 HepG2 cells with serum-free medium were seeded into the upper chamber, and the lower chamber contained the medium with 10 % FBS. The upper chamber was incubated with bacterial *Rhodococcus* CFS powders (Rho) or TSB freeze-dried powders (medium) or PBS (blank control) for 24 h. Then, the chamber membrane was fixed, stained with 0.5 % crystal violet solution, and then observed and photographed under a microscope. For invasion assay, the chamber was coated with Matrigel (BD Biosciences, USA), and the subsequent steps followed the same protocol as the migration assay. Each group was conducted at least 4 biological replicates.

2.9. Tube formation assay

A matrigel-based tube formation assay was performed as previously

described (Aranda and Owen, 2009; Francescone et al., 2011). Briefly, a μ-Slide Angiogenesis (Cat#81506, ibidi, Germany) was coated with 10 μL Matrigel solution (Cat#356234, Sigma, USA) for 30 min at 37 °C before cell culture. Next, 2×10^4 HepG2 cells were harvested and incubated with *Rhodococcus* CFS powders (Rho, dilution in 1:50), TSB freeze-dried powders (medium, dilution in 1:50) and PBS (blank control) in 96-well microplates for 24 h, respectively. Subsequently, the supernatants of co-cultured cells were transferred to the μ-Slide Angiogenesis. Then about 7000 HUVECs were also seeded into μ-Slide Angiogenesis. Each group of cells was tested in three replicated wells. Cells incubation at 37 °C for 8 h, tubule formation was quantified and images were taken under U3ISPM16000KPA industrial digital camera. The ImageJ software was used to count the length of the tube. The angiogenesis index was calculated according to the formula described previously (Aranda and Owen, 2009). Each group was conducted as 5 biological replicates.

2.10. Mouse

C57BL/6 (B6) mice were purchased from Animal Core Facility of Nanjing Medical University. They were kept in a specific pathogen-free (SPF) facility under controlled 22 °C temperature, 55 % humidity and a 12 h light/dark photoperiod. Food and water were provided ad libitum. To minimize potential confounders, all mouse models were all established respectively by the same person. For each model, four different researchers were involved in the blinded procedure. The first researcher randomized the mice according to the random number table method. The second researcher was responsible for building different mouse model. Finally, the third and fourth researchers, who were unaware of the grouping, collected samples, measured, and evaluated the results. To ensure statistical independence, each mouse was treated as an experimental unit. Mice were euthanized by sodium pentobarbital and cervical dislocation. The mice experiments and protocols were reviewed and approved by the Nanjing Medical University Institutional Animal Care and Use Committee (IACUC-2006016).

2.11. Tail vein injection model

To evaluate whether *Rhodococcus* sp. *B513* could colonize the liver, *Rhodococcus* sp. *B513* were injected via tail vein. Eight-week-old male mice were randomly divided into two groups: a control group (Con, $n = 5$) and a *Rhodococcus*-infected group (Rho, $n = 8$) mice began to die by day 21 post-inoculation, thus all mice were euthanized on day 20. The liver, spleen and lung were aseptically collected and placed in separate sterile glass tissue grinders contained PBS. Organ homogenates (0.1 g liver, whole spleen, whole kidney, respectively) were serially diluted in 1 mL sterile PBS, and gradient dilutions were plated on TSA medium to quantify orange-salmon colony forming units (CFU). Plates were incubated at 37 C for 48 h in triplicate, after which orange-salmon colonies were recorded. Results were expressed as the values (mean ± standard error) of $\log_{10}$ *Rhodococcus* sp. *B513* per 1 g of organ.

2.12. Induction of chronic Rhodococcus infection in DEN-induced HCC model

To induce primary HCC, two-week-old male C57BL/6 mice received an intraperitoneal (i.p.) injection of diethylnitrosamine (DEN) (20 mg/kg). Three weeks later, mice were administered weekly i.p. injections of carbon tetrachloride (CCl_4) (25 mg/kg, dissolved in mineral oil) for 9 weeks, as previously described (Uehara et al., 2014). Mice were randomly divided into three groups ($n = 10$ mice per group). Rho group: mice were orally gavaged with *Rhodococcus* sp. *B513* (1×10^9 CFU, 200 uL suspension in PBS) every two days throughout the experiment. Con group: mice received PBS alone as a control. ABX group: Following *Rhodococcus* sp. *B513* treatment at 14 weeks of age, mice were administered a broad-spectrum antibiotic cocktail (vancomycin 0.5 mg/mL, neomycin 1 mg/mL, metronidazole 1 mg/mL, and ampicillin 1 mg/mL) in drinking water until euthanasia, as previously described (Yoshimoto et al., 2013). Following DEN and CCl_4 treatment, all mice developed liver tumor at 5-month-old. Liver tumor and body weight were measured at sacrifice.

2.13. H22 cell line-derived subcutaneous xenograft (CDX) tumor model

Seven-week-old male C57BL/6 mice were randomly allocated into four groups ($n = 10$–11 mice per group). Exponentially growing H22 cells (1×10^5 cells in 100 μL PBS) were subcutaneously injected (s.c.) into the right flank of each mouse. The treatment groups were designed as follows: CDX-Rho group, tumor-bearing mice received oral gavage of *Rhodococcus* sp. *B513* (1×10^9 CFU in 200 μL PBS) every two days; CDX group, control mice received PBS only; Rho group, non-tumor-bearing mice received *Rhodococcus* sp. *B513* (1×10^9 CFU in 200 μL PBS) every two days; Con group, non-tumor-bearing control received PBS only. The tumor size was calculated every five days which using the formula volume (mm^3) = length × width^2 × 0.5. When the length of tumor reached 1.5 cm, mice were euthanized.

2.14. DSS-induced acute colitis mice model

The dextran sulfate sodium (DSS) induced colitis model is a well-established, reproducible that develops independently of T or B cell responses (Oh et al., 2014). Notably, gut microbiomes have been implicated in the development of this colitis variant. Ten 7-week-old male C57BL/6 mice were randomly divided into two groups ($n = 5$ mice per group). Acute colitis was induced by administering 3 % (w/v) DSS in drinking water ad libitum for 7 days, followed by a 3-week recovery period with regular water (DSS group), as previously described (Dieleman et al., 1998; Oh et al., 2014). The DSS-Rho group received *Rhodococcus* sp. *B513* after DSS-treatment for additional 23 days. Body weight was monitored every three days.

2.15. Histological processing and analysis

Whole spleens, livers, and colon were harvested. Organ indices (spleen and liver) were calculated as the organ weight-to-body weight ratio. The distal colon or liver tissues were fixed in 4 % paraformaldehyde for 24 h at 4 °C, then embedded in paraffin. Tissue sections (3–4 μm thickness) were stained with hematoxylin and eosin (HE) staining at Servicebio company (China). The colon histopathology was evaluated from 0 to 14 (total score): crypt hyperplasia, epithelial injury/erosion, inflammation, and percent involvement (Kihara et al., 2003). Histological imaging was captured using a Zeiss Axio Imager 2 Microscope.

2.16. Immunofluorescence staining

The immunofluorescence staining of intestine and live tissues were performed as previously described (Im et al., 2019). Briefly, paraffin-embedded sections were incubated with primary antibodies (diluted 1:200 in 1 % bovine serum albumin-PBS) at 4 °C overnight: rabbit anti-claudin-7 (Cat#A2035, ABclonal, China), rabbit anti-claudin-1 (Cat#BS1063, Bioworld, China), rabbit anti-ZO-1 (Cat#BS71522, Bioworld, China), and rabbit anti-VEGF (Cat#A12303, ABclonal, China). After three times washes with PBS, sections were incubated with Alexa Fluor 488-conjugated goat anti-rabbit IgG secondary antibody (1:2000 dilution; Cat#Z25302, Invitrogen, USA) for 1 hour at room temperature. Fluorescence images were captured by Zeiss LSM 800 Confocal Laser Scanning Microscopy. There were at least four biological replicates in each group.

2.17. Flow cytometry

Tissues samples (spleen, liver, mesenteric lymph nodes (MLN), lamina propria lymphocytes (LPLs), and tumor) were processed for flow cytometry analysis according to the previously described (Huang et al., 2021). Briefly, fresh tissues were mechanically dissociated using gentleMACS Octo Dissociator (Miltenyi Biotec, USA), followed by filtering through 100 μm nylon mesh. For hepatic cells and splenocyte preparations, the red blood cells were lysed by Erthrocytes Lysate (Cat#BL503B, Biosharp, China). All the cells were incubated with the antibody panel for 20–30 min at 4 °C or room temperature. Samples were suspended in PBS for data acquisition on BD FACSVerse using BDVerse software (BD Biosciences, USA). Fluorochrome–conjugated mAb to the following mice antigens were used: CD45-PerCP/Cyanine5.5 (clone 30-F11, Cat#103132), CD3-FITC (clone 17A2, Cat# 100204500), CD4-PE/Cy7 (clone RM4–5, Cat#100528), Foxp3-PE (clone MF-14, Cat#126404), CD25-APC (clone QA19A49, Cat# 162106). Live cells were labelled using the Zombie Aqua fixable viability kit (#423101). All antibodies were purchased from BioLegend.

2.18. DNA extraction and 16S rRNA gene amplicon sequencing

About 100 mg samples (tumor tissues and stool) were used to extract total genome DNA following the protocol of the DNA extraction kit (Cat#DP328 and Cat#DP304 respectively, Tiangen, China). DNA quality and quantity were determined by agarose gel electrophoresis. The concentration and purity of DNA were detected using Qubit 2.0 Fluorometer (Thermo Fisher Scientific, USA). The V4 regions of 16S rRNA were amplified using PCR with the conserved primers 515F (5′-GTGCCAGCMGCCGCGGTAA-3′) and 806R (5′-GGACTACHVGGGTWTCTAAT-3′), and sterile water reaction was used as a negative control. PCR products were purified using the GeneJET Gel Extraction Kit (Thermo Fisher Scientific, USA), then sequenced by Illumina Hiseq 2500 platform (Novogene and Biomarker respectively, China), generating paired-end 250-bp reads.

2.19. Microbiome analyses

Raw sequence data were quality controlled by FLASH v1.2.7, Trimmomatic v0.33, and UCHIME v4.2 software. Bioinformatics analysis of 16S rRNA gene amplicons were performed by QIIME 2.0. Fecal and tumoral samples had a minimum of 68,626 and 22,227 high-quality reads after processing, respectively. Sequences were rarefied to the minimum reads per sample for Alpha-diversity analysis. Alpha diversity (ACE, Chao1, Simpson, and Shannon index) were calculated in Wekemo Bioincloud (https://bioincloud.tech/). Principal coordinate analysis (PCoA) was conducted based on UniFrac and Bray-Curtis distances to visualize amplicon sequence variant (ASV) based bacterial community structures.

The ASVs were assigned to the silva database classifier with $\geq$ 97 % similarity by QIIME 2.0. At each taxonomy level, taxon with relative abundance <0.0001 were filtered out. LEfSe algorithm with default parameters was used to determine significant differentially taxonomy, linear discriminant analysis (LDA) scores $>$ 3 and P value $<$ 0.05 were considered as significant. In order to assess the taxonomic relationship within each group, the top 30 abundant genera were used for co-occurrence network analysis. The co-occurrence patterns were calculated by using Spearman method (correlation coefficient cut-off = 0.5, $P < 0.05$), and visualized with Cytoscape software.

Bacterial functional potential was predicted using PICRUSt2 with default settings (Douglas et al., 2020). Pathways were mapped to Kyoto Encyclopedia of Genes and Genomes (KEGG) orthologs. Differential pathway abundance was assessed using LEfSe algorithm (LDA $>$ 2, P value $<$ 0.05). P values were corrected for multiple comparisons using the Benjamini-Hochberg method to control the false discovery rate (FDR), FDR $<$ 0.05 was considered significant. All 16S rRNA datasets were submitted to CNGB Sequence Archive (CNSA) of China National GeneBank DataBase (CNGBdb) (Accession number CNP0003944 and CNP0003120).

2.20. Statistics

Data distribution normality was evaluated with the one-sample Kolmogorov-Smirnov test. If normality was satisfied, two-tailed Student's t-test was used for two groups analysis. The one-way analysis of variance (ANOVA) was performed for more than two groups. In cases of non-normality, nonparametric tests were applied (Mann-Whitney test for two-group comparison, and Kruskal-Wallis test for comparisons among three or more groups). Results are reported as the mean ± standard deviation (SD). GraphPad Prism software was used to perform the analysis. Significance was defined as: * $P<$ 0.05, ** $P<$ 0.01, *** $P<$ 0.001. The bacterial taxonomic of 16S rRNA analysis between any two groups was conducted using the two-sided Wilcoxon rank-sum test.

3. Results

3.1. Altered composition of microbiota in normal, peritumoral and tumor tissues in HCC patients

To characterize the intratumoral microbiome landscape of HCC, we performed 16S rRNA sequencing on surgically resected liver tissues (tumor, peritumoral and non-tumoral normal tissue) from eight HCC patients. Taxonomic profiling at the ASV level revealed the lowest bacterial abundance in normal tissues (Fig. 1A). The alpha diversity demonstrated marked ecological simplification in tumoral microbiomes, as evidenced by reduced ACE, Chao1 and Shannon index (Fig. 1B, C, D). Differential analysis at genus level revealed similar microbiota composition between normal and peritumoral tissues, such as *Escherichia-Shigella, Rummeliibacillus, Lysinibacillus*, and *Clostridium_sensu_stricto_1* (Fig. 1E, F).

To resolve ecological interactions within hepatic microbiota, we constructed a genus-level correlation-based network in each group (Fig. 1G, H, I). Tumor microbiome demonstrated reduced network complexity with balanced positive and negative correlations (Fig. 1I). Conversely, non-malignant networks displayed predominantly positive interactions (Fig. 1G, H), suggesting cooperative metabolic dependencies in healthy hepatic microbiota.

LEfSe identification of taxonomic biomarkers revealed four bacterial genera significantly associated with tumor, including *Rhodococcus, Enhydrobacter, Corynebacterium_1* and *Micrococcus* (Fig. 1J). Notably, *Rhodococcus* was the most significant tumor-enriched genus, suggesting a potential role of *Rhodococcus* in HCC progression.

3.2. Isolation and phenotypic characterization of Rhodococcus sp. B513 from HCC tissues

To explore the functional relevance of *Rhodococcus* in HCC progression, we performed targeted bacterial isolated from tumoral specimens of an independent validation cohort (10 HCC patients). Freshly resected liver tissues were cultured on TSA medium to isolate *Rhodococcus*. It was aerobic, immobile, formed orange-salmon pigmented colonies, and eventually generated filamentous organisms in liquid culture (Fig. S1A). Microscopic examination of Gram-stained preparations revealed pleomorphic rods exhibiting variable morphology ranging from coccobacilli to branched filaments, consistent with *Rhodococcus* genus characteristics (Fig. S1B). The isolate, designated *Rhodococcus* sp. *B513* (Rho), had the closet genetic relationship with *Rhodococcus aetherovorans* and *Rhodococcus ruber* (Fig. S1C).

Given the reported ability of a *Rhodococcus* species, *Rhodococcus equi*, can survive in host macrophage (Hondalus and Mosser, 1994; Vail et al., 2021), we investigated the interaction between *Rhodococcus* sp. *B513* and macrophages using fluorescence-based assays (Wang et al.,

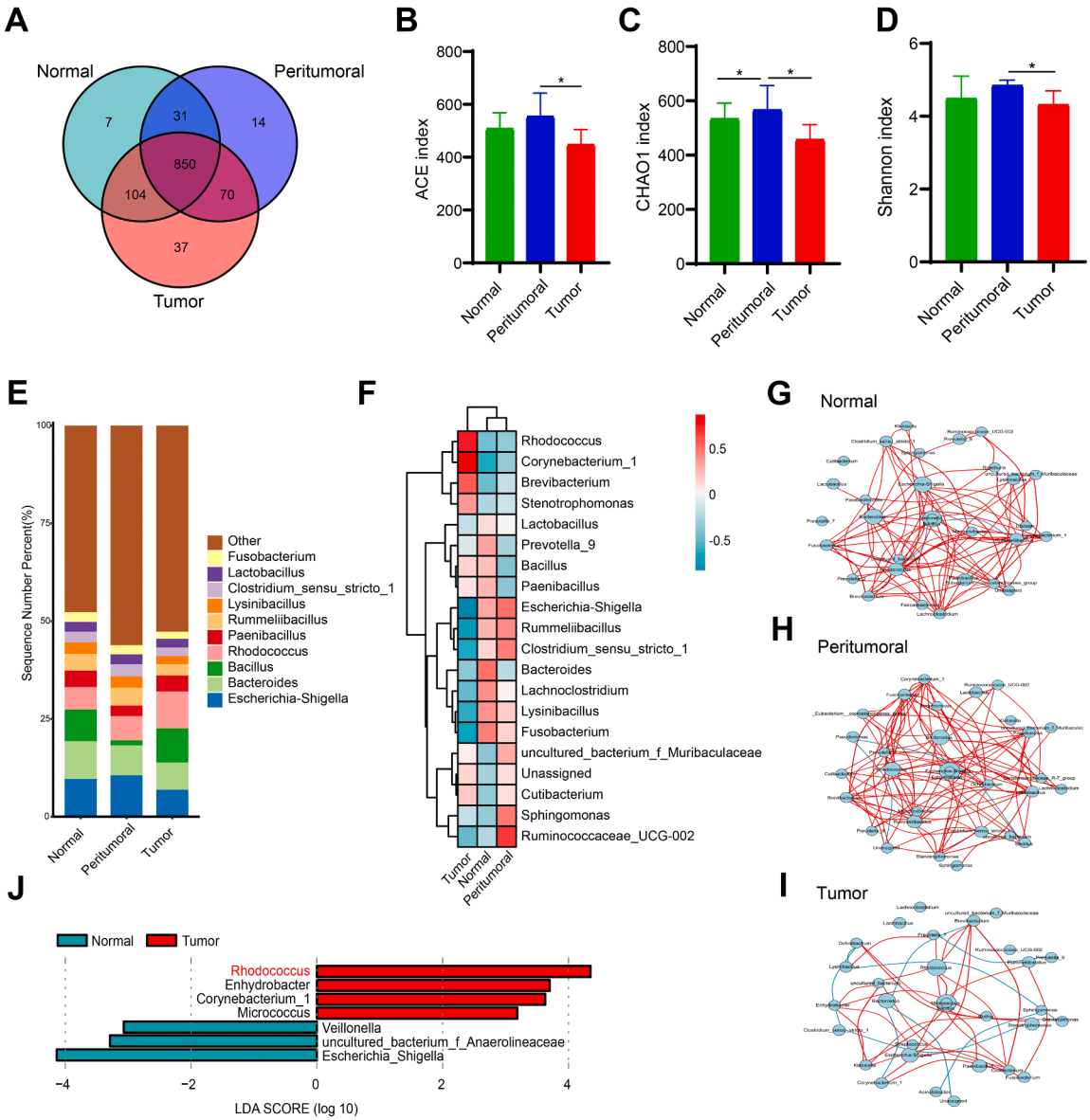

Fig. 1. Bacterial analysis among normal, peritumoral and tumor tissues in HCC patients.
a. Venn diagram of ASVs abundance was performed (n = 8 tissues per group). b-d. The alpha diversity indices of ACE (b), CHAO 1 (c) and Shannon index (d). e. Relative abundance of top 10 genera. f. Heatmap of top 20 genera. g-i. Correlation network of top 30 genera in normal tissues (g), peritumoral tissue (h) and tumor tissues (i). The correlation coefficient was calculated with Spearman's rank test (correlation coefficient cut-off = 0.5, $P < 0.05$). j. Discriminating genus between the normal and tumor tissues by LEfSe analysis. Genus with LDA scores > 3 is shown. *FDR < 0.05, Wilcoxon rank-sum test.

2019). Confocal microscopy revealed efficient phagocytosis at 4 h post-infection (Fig. S1D). Antibiotic susceptibility testing revealed its sensitivity to multiple antibiotics, such as vancomycin, streptomycin, kanamycin, and spectinomycin (Table S1). The results implicated that the intratumoral bacterium *Rhodococcus B513*-a phagocytosis-resistant strain, with closely related to *Rhodococcus* species, which provided a tractable model for investigating tumor-microbe interactions.

3.3. Systemic dissemination and hepatic colonization of *Rhodococcus* sp. *B513*

To evaluate the systemic pathogenicity and organotropism of *Rhodococcus* sp. *B513*, we established a murine infection model using 8-week-old C57BL/6 J mice. Following tail vein injection of *Rhodococcus* sp. *B513* or sterile PBS control, serial physiological and microbiological assessments were performed at the 21-day (Fig. 2A). *Rhodococcus* sp. *B513*-injected mice exhibited progressive weight loss (Fig. 2B), accompanied by significant increased weight ratio of liver, spleen, kidney, and lung (Fig. 2C). Notably, 62.5 % of *Rhodococcus*-infected mice developed hepatic abscesses characterized by marked central suppurative inflammation surrounded by fibrin and necrosis (Fig. 2D, E, Table S2). Quantitative culture of homogenized tissues revealed rapid hepatic colonization, with liver CFU counts reaching 2.16×10^{10} CFU/mL post injection (Table S2). The results strongly suggested that *Rhodococcus* sp. *B513* was able to colonize in liver tissues after intravenous injection in adult mice.

3.4. *Rhodococcus sp. B513 promoted hepatocellular carcinoma growth and progression*

To define the functional role of *Rhodococcus* sp. *B513* in HCC, we performed transwell assays using HepG2 cells treated with *Rhodococcus*

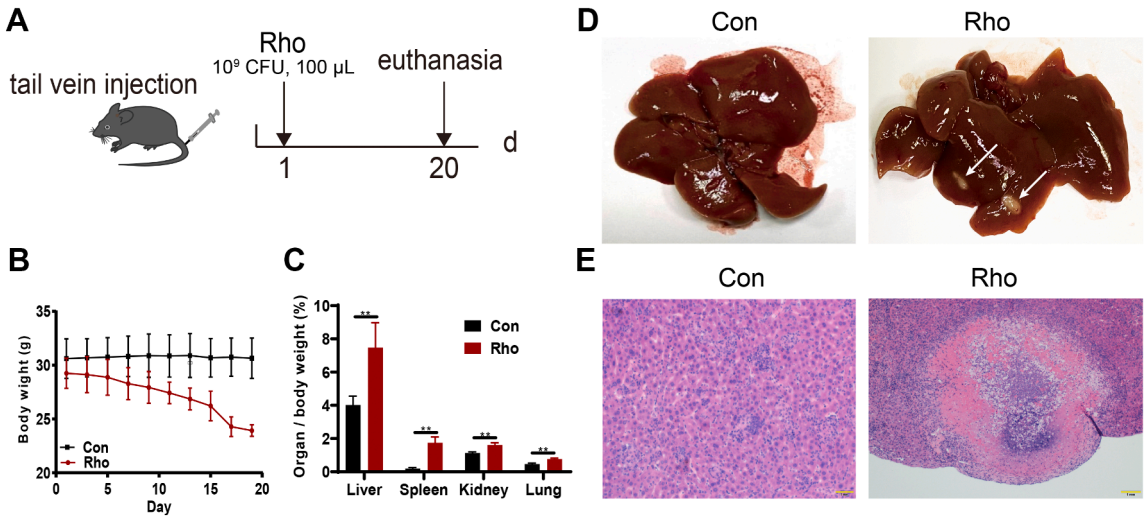

Fig. 2. Effect of *Rhodococcus* sp. *B513* administration on the tail vein injection model. a. Schematic representation of the experiment design. Eight-week-old male mice were injected with *Rhodococcus* sp. *B513* (Rho, $n = 8$ mice) or PBS (Con, $n = 5$ mice) via tail vein. b. Body weight was measured. c. Organ weight relative to body weight. $^{*}p < 0.05$, $^{**}p < 0.01$, unpaired two-tailed Student's *t*-tests with Mann-Whitney test. d. Representative macroscopic photographs of livers. White arrow indicates the hepatic abscess. e. Representative HE staining of liver sections.

CFS powders (Fig. 3A). Treated cells exhibited significantly enhanced migration and invasion capabilities compared to controls (Fig. 3A). Given the established involvement of angiogenesis in HCC pathogenesis, we further assessed the pro-angiogenic potential of *Rhodococcus* CFS. Treatment markedly stimulated tube formation in HUVECs (Fig. 3B).

To validate these findings *in vivo*, we established a DEN/CCl_4-induced HCC model (Fig. 4A). Mice were treated with *Rhodococcus* sp. *B513* (Rho group) developed significantly more hepatic tumor nodules than controls, particularly those >5 mm in diameter (Fig. 4B, C). Next, we applied antibiotics to remove bacteria (ABX group). The antibiotic-treated mice exhibited cecal enlargement (Fig. S2A), consistent with prior observations (Yoshimoto et al., 2013). And the ABX-treatment alleviated the *Rhodococcus* sp. *B513*-driven tumor progression (Fig. 4B, C, D), supporting a causal role for *Rhodococcus* sp. *B513*. The Rho group also exhibited increased liver-to-body weight ratios (Fig. 4D) and severe intestinal inflammation (Fig. 4E). In addition, species-specific PCR confirmed bacterial translocation to the liver (Fig. S2B).

Then, we investigated whether gut barrier disruption mediated *Rhodococcus* sp. *B513*'s pro-tumorigenic effects. Tight junction proteins are critical for intestinal barrier integrity (Xing et al., 2020). Strikingly,

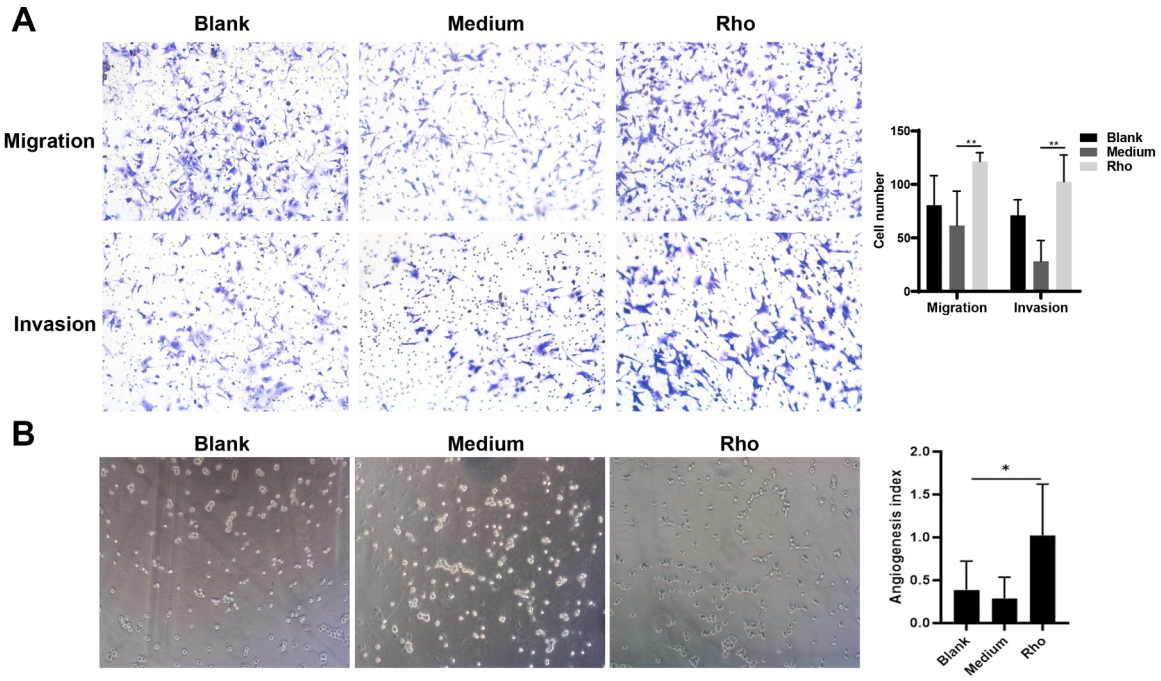

Fig. 3. Effect of *Rhodococcus* sp. *B513* on the viability of cells in vitro. a. Transwell assay analysis of HepG2 cell migration and invasion were treated with cell-free supernatant of *Rhodococcus* sp. *B513* (Rho) or TSB medium (Medium) treatment, and PBS as the blank, $n = 4$–5 biological replicates/group. $^{**}p < 0.01$, one-way ANOVA test with Kruskal-Wallis test. b. HUVECs cultures were treated with supernatants from HepG2 (Blank), supernatants from HepG2 infected with cell-free supernatant of *Rhodococcus* sp. *B513* (Rho), TSB treatment (Medium) for 8 h and then subjected to tube formation assay, respectively, $n = 4$–5 biological replicates/group. $^{*}p < 0.05$, one-way ANOVA test.

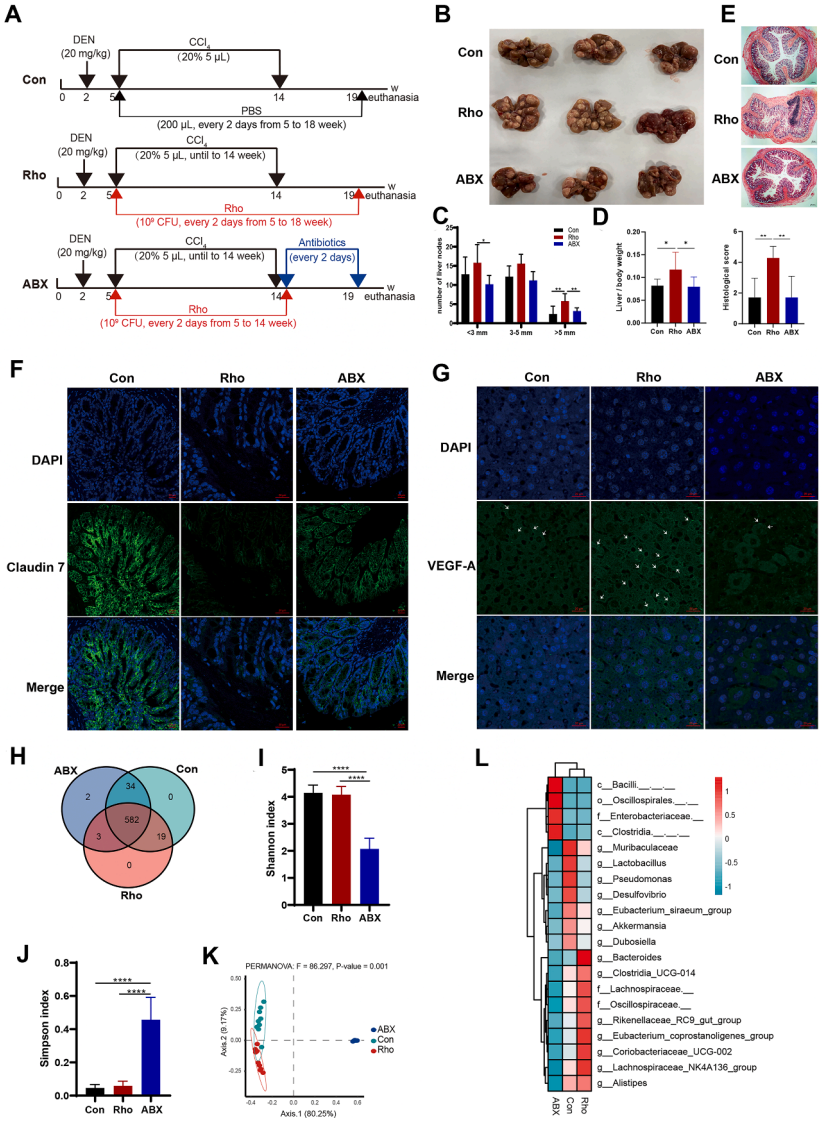

Fig. 4. Effect of *Rhodococcus* sp. *B513* administration on chemical-induced HCC model. a. Schematic representation of the experiment design. Two-week-old male mice injected with DEN. Then, mice were received 9 weekly injection of CCl_4 (Con), or gavaged with *Rhodococcus* sp. *B513* (Rho). In addition, mice were oral gavage by antibiotics cocktail at week 14 until euthanized (ABX). b. Photograph of tumor. c. Quantification of tumor number ($n = 8$ mice/group), one-way ANOVA test with Kruskal–Wallis test. d. Liver weight relative to body weight ($n = 8$ mice/group), one-way ANOVA test with Kruskal–Wallis test. e. HE staining and histological score of colons, $n = 7$ mice/group, one-way ANOVA test with Kruskal–Wallis test. f. Immunofluorescence staining of claudin-7 protein in colon tissue, $n = 4$–5 mice/group. g. Immunofluorescence staining of VEGF-A protein in liver tissue, arrow indicates the VEGF-A, $n = 4$–5 mice/group. h. Venn diagram of ASVs abundance was performed, $n = 9$–10 mice/group. i-j. The alpha diversity of Shannon (I) and Simpson (J) index, one-way ANOVA test. k. PCoA of bacterial beta diversity based on the unweighted UniFrac distances. l. Heatmap of top 20 genera.
$^*p < 0.05$, $^{**}p < 0.01$, $^{***}p < 0.001$, $^{****}p < 0.0001$.

administration of *Rhodococcus* sp. *B513* downregulated key barrier proteins (claudin-1, claudin-7, and ZO-1; Fig. 4F, Fig. S2C, S2D), indicating compromised gut integrity that permits bacterial translocation to the liver, which is consistent with our detection of *Rhodococcus* DNA in hepatic tissue. Within the liver microenvironment, translocated bacteria or their components subsequently upregulated hepatic VEGF-A (Fig. 4G), a key angiogenesis mediator known to fuel HCC growth. Previous studies have reported that *Rhodococcus* were enriched in intestinal mucosa in inflammatory bowel disease patients (Wang et al., 2022). Consistent with this clinical associations between *Rhodococcus* and mucosal inflammation, we also observed that *Rhodococcus* sp. *B513* exacerbated intestinal pathology in a DSS-induced acute colitis model (Fig. S3). Collectively, these data suggested that *Rhodococcus* sp. *B513* disrupts intestinal barrier integrity, promotes VEGF-driven angiogenesis, and ultimately accelerates HCC progression.

3.5. *Rhodococcus sp. B513 exacerbated gut dysbiosis in DEN-induced HCC model*

To assess the impact of *Rhodococcus* sp. *B513* on the gut microbiota in HCC, we conducted 16S rRNA gene sequencing on fecal samples. No unique ASVs were detected between the Control (Con) and *Rhodococcus* (Rho) groups (Fig. 4H). Alpha diversity, measured by the Shannon and Simpson indices, was significantly different in the ABX group compared to both the Con and Rho groups (Fig. 4I, J). PCoA revealed significant compositional differences among the three groups (Fig. 4K, Fig. S4A).

Differential abundance analysis at the phylum and genus levels identified significant taxon alteration (Fig. S4B, S4C, S4D). Significant alterations in the top 20 genera were observed in the Rho group compared to Controls (Fig. 4L, Fig. S4E). Notably, this dysbiosis was characterized by a significant depletion of short-chain fatty acids-

producing (SCFA) producing bacteria, including the diminished genera *Muribaculaceae, Lactobacillus, Akkermansia*, and *Dubosiella*. Additionally, the pro-inflammatory bacteria (e.g., *Bacteroides, Rikenellaceae RC9, Colidextribacter, Turicibacter* and *Coriobacteriaceae UCG-002*) were enriched following *Rhodococcus* sp. *B513* administration. Furthermore, co-occurrence network analysis revealed substantially simpler microbial interactions within the Rho group (Fig. S4F, S4G, S4H), mirroring the reduced network complexity observed in tumor tissue from HCC patients (Fig. 1I). This diminished interconnectivity suggests that *Rhodococcus* sp. *B513* disrupts the compositional balance and ecological complexity of the gut microbiota.

To investigate the biological function of microbiota induced by *Rhodococcus* sp. *B513*, we used PICRUSt2 to assess the potential function of microbiome (Fig. S5). Of note, twelve metabolism pathways related with sugar metabolism (green in colour) were increased in the Rho group, meanwhile, the antibiotic biosynthesis pathways were also enriched (blue in colour). In addition, Rho group also showed an enrichment in pathways linked to inflammatory diseases, including NOD-like receptor signaling.

3.6. *Rhodococcus sp. B513 accelerated tumor progression in H22 CDX tumor model*

To evaluate the direct tumorigenic effects of *Rhodococcus* sp. *B513*, we established a H22 CDX tumor model with oral *Rhodococcus* sp. *B513* administration (Fig. 5A). The results indicated that *Rhodococcus* enhanced tumor growth and burden compared to controls (Fig. 5B, C). Histopathological analysis revealed enhanced epithelial damage in treated mice, characterized by extensive colonic gland dysplasia (Fig. 5D).

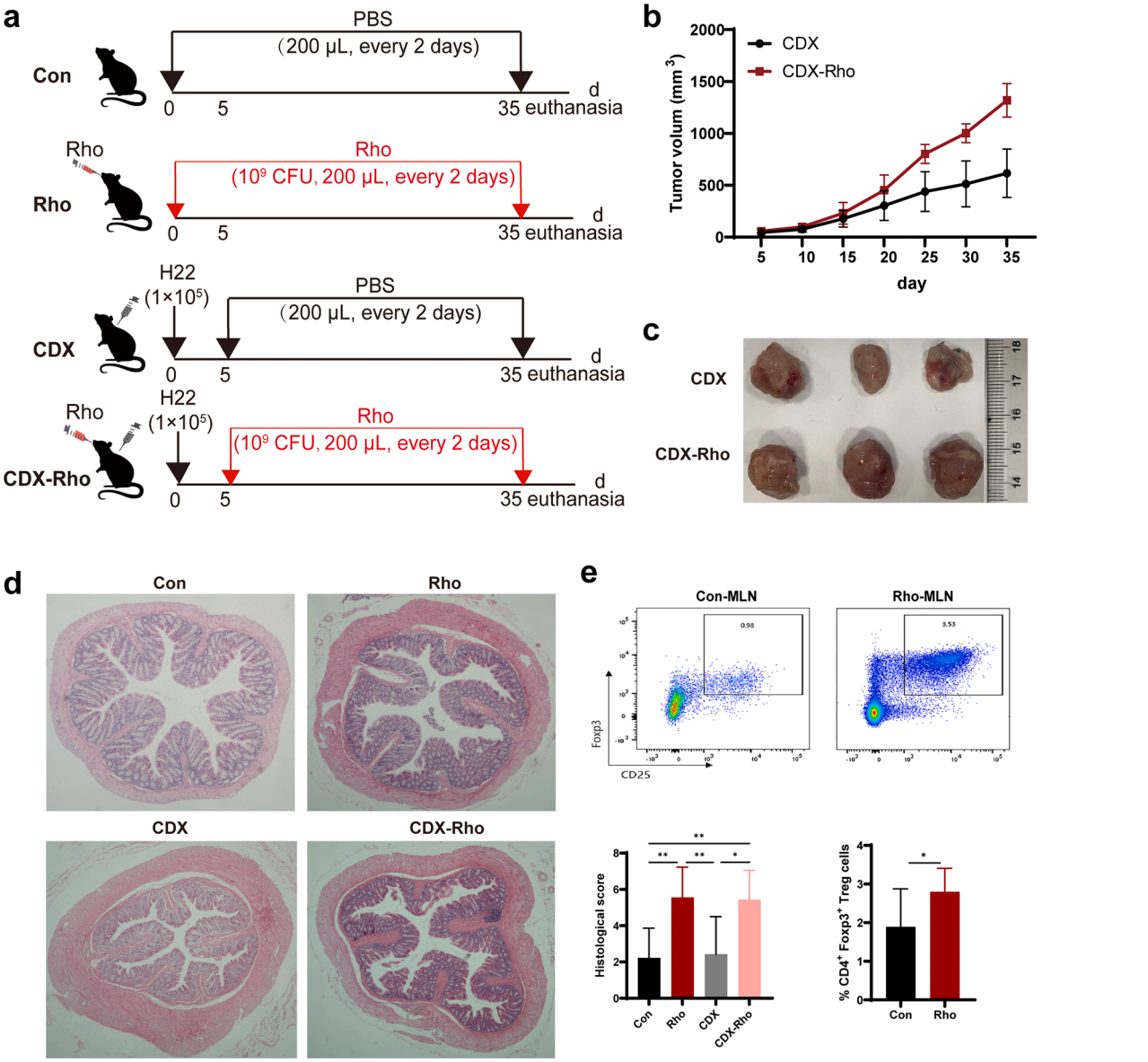

Fig. 5. Effect of *Rhodococcus* sp. *B513* administration on H22 subcutaneous xenograft tumor model. a. Schematic representation of the experiment design. Eight-week-old male C57BL/6 mice were subcutaneous injected with H22 cells derived xenograft (CDX). Mice were orally gavage with PBS (CDX) or *Rhodococcus* sp. *B513* (CDX-Rho). Mice were gavaged with *Rhodococcus* sp. *B513* throughout the experiment (Rho), while mice were received PBS as the control group (Con), n = 10–11 mice/group. b. The curve of tumor volume. c. Representative images of tumor. d. HE staining and histological score of colons (Con, $n = 9$; Rho, $n = 9$; CDX, $n = 7$; CDX-Rho, $n = 9$), one-way ANOVA test.e. Identification of $CD4^{+}$Treg cells in mesenteric lymph nodes (MLN) tissues (Con, $n = 7$; Rho, $n = 8$), unpaired 2-tailed t-test.
$^{*}p < 0.05$, $^{**}p < 0.01$.

Flow cytometry analysis of immune cells (Th17, Treg, macrophage, $CD8^+$ and $CD4^+$) within spleen, liver, MLN, LPLs, and tumor tissues, and identified a specific enrichment of $CD4^+Foxp3^+$ Treg cells exclusively in MLNs of *Rhodococcus*-treated mice (Fig. 5E). This finding aligns with established reports linking $Foxp3^+$Treg dysregulation to inflammatory bowel disease (Ramanan et al., 2023), and correlates with our observed histopathological alterations (Fig. 5D). Collectively, these results indicated that *Rhodococcus* sp. *B513* drive intestinal inflammation through modulation of the local immune microenvironment, thereby accelerating tumor progression.

4. Discussion

Increasing evidences indicated intratumoral microbe could exert a more direct and localized influence on tumor progression than gut microbes. Previous studies with large sample sizes have confirmed the presence of intratumor bacteria in tumor and immune cells, demonstrating that the intratumoral bacteria are tumor specific (Nejman et al., 2020; Galeano Niño et al., 2022). These microbes have been indicated to interact with tumor cells in various cancer types, including brain, bone, breast, lung, colorectal, and skin cancers (Nejman et al., 2020; Fu et al., 2022; Goto et al., 2023). Consequently, understanding whether and how intratumor bacteria contribute to tumorigenesis, progress, and targeted necessitates further investigation.

However, characterization of the intratumor microbiome of HCC remains limited. Till now, several intratumor bacteria, including *Streptococcaceae, Lactococcus, Cutibacterium, Stenotrophomonas maltophilia, Staphylococcus capitis, Paraburkholderia fungorum, Klebsiella pneumoniae* (Losic et al., 2020; Komiyama et al., 2021; Huang et al., 2022; Sun et al., 2023a; Liu et al., 2024; Wang et al., 2025)., have been suggested as markers for cirrhosis or intrahepatic cholangiocarcinoma or HCC. These findings indicated heterogeneity in the intratumoral microbiota across different hepatic cancer subtypes, mutation states, and invasion degree. Thus, a more in-depth analysis of the intratumoral microbiome in a larger cohort of HCC patients is warranted.

Here we observed that a simper intratumoral bacteria interaction in HCC patients, and identified enrichment of *Rhodococcus* sp. *B513* in tumor tissues. *Rhodococcus* sp. *B513* aggravated the tumor growth via facilitating intestinal inflammation, inducing microbiome dysbiosis, and activating VEGF pathway. Genus *Rhodococcus* belongs to the phylum *Actinobacteria* and is widely distributed in nature. It exhibited remarkable adaptability to environmental stress, including extreme conditions such as antibiotics exposure (Mohadeseh et al., 2018). And multidrug-resistant *R. equi* had been widely detected in the United States (Mohadeseh et al., 2018). Interestingly, functional prediction in our study indicated that *Rhodococcus* sp. *B513* may enhance antibiotic accumulation and glycometabolism (Fig. S5). In addition, *Rhodococcus* species are known to form antibiotic-resistant biofilm in polyurethane catheters of indwelling central venous catheters (Al Akhrass et al., 2012). Collectively, these properties suggested that *Rhodococcus* infection may pose significant challenges for anti-bacterial therapy.

Notably, *Rhodococcus* was also reported as the most dominant genus in tumor tissues of HCC patients (Sun et al., 2023b). Meanwhile, *Rhodococcus* was also enriched in bile samples from the liver transplantation patients with biliary complication (Ferreira et al., 2018). In addition, *Rhodococcus* species were frequently found residing in the intestinal mucosa as commensals in gestational diabetes mellitu, ulcerative colitis, and gastric carcinoma patients (Wang et al., 2019; Su et al., 2021; Zhao et al., 2021). This evidence supported the hypothesis that translocation of *Rhodococcus* from the intestine to the liver likely contributes to HCC progression.

HCC often involves the multi etiopathogenetic factors of participation. Recent evidences emphasized the significant role of intestinal dysbiosis in HCC progression. In our HCC model, administration of *Rhodococcus* sp. *B513* disrupted microbiota homeostasis and reduced bacterial network complexity (Fig. 4, Fig. S4). Notably, the SCFA-producing bacteria (e.g., *Akkermansia, Dubosiella, Muribaculaceae* and *Lactobacillus*) were significantly depleted in the Rho group. Among these bacteria, *Muribaculaceae* was associated with longevity (Sibai et al., 2020), while probiotics like *Lactobacillus* and *Akkermansia* were known to restore the intestinal barrier, reduce mucosal inflammation, and attenuate liver inflammation and fibrosis (Neyrinck et al., 2019; Zhao et al., 2020; Rao et al., 2021). SCFAs serve as the primary energy sources for colonic enterocytes and are essential for maintaining the integrity of intestinal barrier. Consequently, the reduction in SCFA-producing bacteria likely impairs intestinal barrier integrity, potentially enabling gut microbes translocate to the liver and contributing to HCC progression.

Another significant change was the increases of pro-inflammatory bacteria (e.g., *Bacteroides, Rikenellaceae RC9, Colidextribacter, Turicibacter* and *Coriobacteriaceae UCG-002*) following *Rhodococcus* sp. *B513* administration. Notably, *Bacteroides* has been identified as intratumoral bacteria that strongly promote tumor growth and metastatic progression in colorectal cancer (Chung et al., 2018; Cao et al., 2021). Similarly, *Colidextribacter* was also observed enrichment across liver fibrosis severities in DEN/CCl_4-induced model (Xiang et al., 2022), and showed positive correlation with peroxidation marker (e.g., MDA) but negative correlation with serum antioxidant capacity (Wang et al., 2021). Furthermore, elevated abundance of *Colidextribacter, Turicibacter, Rikenellaceae RC9* and *Coriobacteriaceae UCG-002* were documented in high-fat diet (HFD) induced hepatitis model (Sun et al., 2022; Yan et al., 2022). These bacteria were strongly associated with impaired hepatic function and disease progression. Collectively, *Rhodococcus* sp. *B513* administration in the HCC model increased pro-inflammation bacteria and decreased SCFA-producing bacteria, consistently linked with HCC advancement.

Alterations in the intestinal microbiota may influence metabolic dysregulation in HCC. Functional analysis revealed that *Rhodococcus* sp. *B513* modulates multiple metabolic pathways, including glycan degradation, lipoic acid metabolism, cyanoamino acid metabolism, especially the sugar metabolism and antibiotics biosynthesis (Fig. S5). This finding was significant given that most solid tumor cells presented Warburg effect, adapting to their hypoxic microenvironment by preferentially utilizing aerobic glycolysis for energy production (Icard et al., 2018). Current HCC therapies were primarily target angiogenic pathways, especially VEGF-mediated tumor angiogenesis (Kuzuya et al., 2011). Intriguingly, trehalose 6,6′-dimycolate (TDM), a characteristic cell wall component of mycolic acid-containing bacteria including *Rhodococcus*, has been demonstrated to augment VEGF production and promote neovascularization in granulomatous tissue (Sakaguchi et al., 2000). Given the significant enrichment of *Rhodococcus* sp. *B513* in tumor tissues and its distinct metabolic profile, we hypothesized that *Rhodococcus* may exert carcinogenesis through metabolites in the tumor microenvironment. Future studies should identify the specific *Rhodococcus*-derived metabolites involved and elucidate their underlying molecular mechanisms in HCC pathogenesis.

The origin of hepatic intratumoral microbiome represents a critical research focus. Accumulating evidences have illustrated that periodontitis pathogenic bacteria including *Porphyromonas gingivalis, Aggregatibacter actinomycetemcomitans, Streptococcus noxia* can influence liver diseases pathophysiology via blood hematogenous or enteral dissemination (Albuquerque-Souza and Sahingur, 2022). Notably, clinical researched have revealed that intratumoral *Mycoplasma hyorhinis* could undergo retrograde hepatic infection via the oral-duodenal-hepatopancreatic ampulla route, implying significant crosstalk between intratumoral and oral microbiota (Qiao et al., 2023). The crosstalk mechanism among oral, intestinal, and intratumoral microbes may facilitate hepatic-intestinal circulation. Specifically, microbiotal dysregulation increases intestinal permeability and promotes bacterial translocation. Furthermore, bacteria and their metabolites can accelerate bacterial translocation across the intestinal barrier via the mesenteric lymph system (Yu et al., 2022). Moreover, *Rhodococcus* species had a propensity to cause liver abscesses, potentially through

intestinal tract (Prescott, 1991). Thus, further comprehensive studies are required to elucidate the microbial transport processes and their underlying mechanism in HCC.

It was really challenge to precisely modulate intratumor microbiota in clinical practice. However, a recent clinical trial in HCC patients demonstrated that administration of a bacterial cocktail containing *Bifidobacterium longum* significantly shortened hospital duration and improved overall 1-year survival rates (Yu et al., 2024). Recent clinical studies have documented that antibiotic use during immune checkpoint inhibitor (ICI) therapy with increased mortality in HCC patients (Pinato et al., 2019; Cheung et al., 2021). By contrast, preclinical evidence demonstrates that antibiotics treatment dramatically reduce secondary bile acids accumulation, resulting insignificantly suppressed tumor progression in NASH-associated HCC (Yamada et al., 2018). The clinical application of antibiotics for targeting intratumoral microbiota remains challenging due to variations in dysbiosis effects, drug absorption efficiency, cell permeability and bacterial resistance profiles. Consequently, researchers have explored personalized phage cocktails as an alternative approach for microbiome modulation in cancer therapy (Kabwe et al., 2021; Hatfull et al., 2022). Nevertheless, bacteriophages are best utilized as a complement for antibiotics, or last-line therapy when standard treatments fail. Despite the complex crosstalk between microbiota and tumour, targeted modification of intratumoral microbiota represents a promising therapeutic strategy for cancer treatment.

5. Conclusion

In conclusion, we characterized tumor-associated microbiota of HCC using a pilot cohort and identified pro-tumorigenic role of *Rhodococcus* sp. *B513* in HCC progression. Based on the current data, the precise relationship between *Rhodococcus* abundance and clinical features requires further elucidation. Future investigations are required to focus on the *Rhodococcus*-derived metabolites and molecular mechanisms in hepatocarcinogenesis. While, we believe that our findings provide a basis and guidance for further research on intratumoral microbiota in HCC.

CRediT authorship contribution statement

Qisha Liu: Conceptualization, Data curation, Formal analysis, Funding acquisition, Investigation, Methodology, Software, Validation, Visualization, Supervision, Writing – original draft, Writing – review & editing. **Jingjing Wang:** Writing – original draft, Conceptualization, Investigation, Methodology, Validation. **Yutong Yao:** Data curation, Validation, Writing – review & editing. **Xuqi Sun:** Funding acquisition, Resources, Investigation, Methodology. **Weijia Fang:** Resources, Project administration. **Yewei Zhang:** Resources. **Zhi Liu:** Conceptualization, Data curation, Validation, Writing – review & editing, Formal analysis, Methodology, Software. **Yi Zheng:** Funding acquisition, Resources, Supervision, Writing – review & editing, Project administration, Conceptualization.

Declaration of competing interest

The authors declare that they have no known competing financial interests or personal relationships that could have appeared to influence the work reported in this paper.

Acknowledgements

We thank Prof. Wei Wang provided fluorescent D-amino acid (FDAA) probes to us. This work was supported by National Natural Science Foundation of China (NSFC) grants 31900123 and 82202875 to QL and XS, Zhejiang Provincial Natural Science Foundation LY21H160029 to YZ.

Supplementary materials

Supplementary material associated with this article can be found, in the online version, at doi:10.1016/j.crmicr.2025.100428.

Data availability

Data will be made available on request.

References

Al Akhrass, F., Al Wohoush, I., Chaftari, A.M., et al., 2012. *Rhodococcus* bacteremia in cancer patients is mostly catheter related and associated with biofilm formation. PLoS. One 7, e32945. https://doi.org/10.1371/journal.pone.0032945.

Albuquerque-Souza, E., Sahingur, S.E., 2022. Periodontitis, chronic liver diseases, and the emerging oral-gut-liver axis. Periodontol. 2000 89, 125–141. https://doi.org/10.1111/prd.12427.

Aranda, E., Owen, G.I., 2009. A semi-quantitative assay to screen for angiogenic compounds and compounds with angiogenic potential using the EA.hy926 endothelial cell line. Biol. Res. 42, 377–389. https://doi.org/10.4067/S0716-97602009000300012.

Cao, Y., Wang, Z., Yan, Y., et al., 2021. Enterotoxigenic *Bacteroides fragilis* promotes intestinal inflammation and malignancy by inhibiting exosome-packaged mir-149-3p. Gastroenterology 161, 1552–1566. https://doi.org/10.1053/j.gastro.2021.08.003.

Chai, X., Wang, J., Li, H., et al., 2023. Intratumor microbiome features reveal antitumor potentials of intrahepatic cholangiocarcinoma. Gut. Microbes. 15, 2156255. https://doi.org/10.1080/19490976.2022.2156255.

Cheung, K.S., Lam, L.K., Seto, W.K., et al., 2021. Use of antibiotics during Immune Checkpoint inhibitor treatment is associated with lower survival in hepatocellular carcinoma. Liver. Cancer 10, 606–614. https://doi.org/10.1159/000518090.

Chung, L., Thiele Orberg, E., Geis, A.L., et al., 2018. Bacteroides fragilis toxin coordinates a pro-carcinogenic inflammatory cascade via targeting of colonic epithelial cells. Cell Host. Microbe 23, 203–214. https://doi.org/10.1016/j.chom.2018.01.007.

Dieleman, L.A., Palmen, M.J., Akol, H., et al., 1998. Chronic experimental colitis induced by dextran sulphate sodium (DSS) is characterized by Th1 and Th2 cytokines. Clin. Exp. Immunol. 114, 385–391. https://doi.org/10.1046/j.1365-2249.1998.00728.x.

Dimitrieva-Moats, G.Y., Ünlü, G., 2012. Development of freeze-dried bacteriocin-containing preparations from lactic acid bacteria to inhibit Listeria monocytogenes and Staphylococcus aureus. Probiotics Antimicrob. Proteins 4, 27–38. https://doi.org/10.1007/s12602-011-9088-1.

Dohlman, A.B., Klug, J., Mesko, M., et al., 2022. A pan-cancer mycobiome analysis reveals fungal involvement in gastrointestinal and lung tumors. Cell 185, 3807–3822. https://doi.org/10.1016/j.cell.2022.09.015 e12.

Douglas, G.M., Maffei, V.J., Zaneveld, J.R., et al., 2020. PICRUSt2 for prediction of metagenome functions. Nat. Biotechnol. 38, 685–688. https://doi.org/10.1038/s41587-020-0548-6.

Ferreira, R.M., Pereira-Marques, J., Pinto-Ribeiro, I., et al., 2018. Gastric microbial community profiling reveals a dysbiotic cancer-associated microbiota. Gut 67, 226–236. https://doi.org/10.1136/gutjnl-2017-314205.

3rd Francescone, R.A., Faibish, M., Shao, R., 2011. A Matrigel-based tube formation assay to assess the vasculogenic activity of tumor cells. J. Vis. Exp.: JoVE 3040. https://doi.org/10.3791/3040.

Fu, A., Yao, B., Dong, T., et al., 2022. Tumor-resident intracellular microbiota promotes metastatic colonization in breast cancer. Cell 185, 1356–1372. https://doi.org/10.1016/j.cell.2022.02.027.

Galeano Niño, J.L., Wu, H., LaCourse, K.D., et al., 2022. Effect of the intratumoral microbiota on spatial and cellular heterogeneity in cancer. Nature 611, 810–817. https://doi.org/10.1038/s41586-022-05435-0.

Goto, Y., Iwata, S., Miyahara, M., et al., 2023. Discovery of intratumoral oncolytic bacteria toward targeted anticancer theranostics. Adv. Sci. (Weinh) 10, e2301679. https://doi.org/10.1002/advs.202301679.

Hatfull, G.F., Dedrick, R.M., Schooley, R.T., 2022. Phage therapy for antibiotic-resistant bacterial infections. Annu. Rev. Med. 73, 197–211. https://doi.org/10.1146/annurev-med-080219-122208.

Hondalus, M.K., Mosser, D.M., 1994. Survival and replication of *RhodococcusRhodococcus equi* in macrophages. Infect. Immun. 62, 4167–4175. https://doi.org/10.1128/iai.62.10.4167-4175.1994.

Huang, J., Song, P., Hang, K., et al., 2021. Sleep deprivation disturbs immune surveillance and promotes the progression of hepatocellular carcinoma. Front. Immunol. 12, 727959. https://doi.org/10.3389/fimmu.2021.727959.

Huang, J.H., Wang, J., Chai, X.Q., et al., 2022. The intratumoral bacterial metataxonomic signature of hepatocellular carcinoma. Microbiol. Spectr. 10, e0098322. https://doi.org/10.1128/spectrum.00983-22.

Icard, P., Shulman, S., Farhat, D., et al., 2018. How the Warburg effect supports aggressiveness and drug resistance of cancer cells? Drug Resist. Updates 38, 1–11. https://doi.org/10.1016/j.drup.2018.03.001.

Im, K., Mareninov, S., Diaz, M.F.P., et al., 2019. An introduction to performing immunofluorescence staining. Methods Mol. Biol. 1897, 299–311. https://doi.org/10.1007/978-1-4939-8935-5_26.

Kabwe, M., Dashper, S., Bachrach, G., et al., 2021. Bacteriophage manipulation of the microbiome associated with tumour microenvironments-can this improve cancer

therapeutic response? FEMS Microbiol. Rev. 45, fuab017. https://doi.org/10.1093/femsre/fuab017.
Kihara, N., de la Fuente, S.G., Fujino, K., et al., 2003. Vanilloid receptor-1 containing primary sensory neurones mediate dextran sulphate sodium induced colitis in rats. Gut 52, 713–719. https://doi.org/10.1136/gut.52.5.713.
Komiyama, S., Yamada, T., Takemura, N., et al., 2021. Profiling of tumour-associated microbiota in human hepatocellular carcinoma. Sci. Rep. 11, 10589, 10.1038/s41598-021-89963-1.
Kuzuya, T., Takeda, K., Utsunomiya, S., et al., 2011. A case of intractable hepatic encephalopathy successfully treated by oral administration of vancomycin hydrochloride, with subsequent improvement of hepatic function reserve enabling transcatheter arterial chemoembolization against hepatocellular carcinoma. Gan Kagaku Ryoho Cancer Chemother. 38, 995–997.
Lin, L., Song, J., Du, Y., et al., 2020. Quantification of bacterial metabolic activities in the gut by D-amino acid-based Invivo labeling. Angew. Chem. Int. Ed. Engl. 59, 11923–11926. https://doi.org/10.1002/anie.202004703.
Liu, B., Zhou, Z., Jin, Y., et al., 2022. Hepatic stellate cell activation and senescence induced by intrahepatic microbiota disturbances drive progression of liver cirrhosis toward hepatocellular carcinoma. J. ImmunOther Cancer 10, e003069. https://doi.org/10.1136/jitc-2021-003069.
Liu, Q., Li, F., Zhuang, Y., et al., 2019. Alteration in gut microbiota associated with hepatitis B and non-hepatitis virus related hepatocellular carcinoma. Gut. Pathog. 11, 1. https://doi.org/10.1186/s13099-018-0281-6.
Liu, Y., Kim, E.S., Guo, H., 2024. Hepatitis B virus-related hepatocellular carcinoma exhibits distinct intratumoral microbiota and immune microenvironment signatures. J. Med. Virol. 96, e29485. https://doi.org/10.1002/jmv.29485.
Liu, Z., Wang, Y., Dou, C., et al., 2018. Hypoxia-induced up-regulation of VASP promotes invasiveness and metastasis of hepatocellular carcinoma. Theranostics 8, 4649–4663. https://doi.org/10.7150/thno.26789.
Losic, B., Craig, A.J., Villacorta-Martin, C., et al., 2020. Intratumoral heterogeneity and clonal evolution in liver cancer. Nat. Commun. 11, 291. https://doi.org/10.1038/s41467-019-14050-z.
Manfredo Vieira, S., Hiltensperger, M., Kumar, V., et al., 2018. Translocation of a gut pathobiont drives autoimmunity in mice and humans. Science 359, 1156–1161. https://doi.org/10.1126/science.aar7201.
Mohadeseh, M., Mehdi, et al., 2018. Current taxonomy of *Rhodococcus* species and their role in infections. Eur. J. Clin. Microbiol. Infect. Dis. 37, 2045–2062. https://doi.org/10.1007/s10096-018-3364-x.
Nejman, D., Livyatan, I., Fuks, G., et al., 2020. The human tumor microbiome is composed of tumor type-specific intracellular bacteria. Science 368, 973–980. https://doi.org/10.1126/science.aay9189.
Neyrinck, A.M., Catry, E., Taminiau, B., et al., 2019. Chitin-glucan and pomegranate polyphenols improve endothelial dysfunction. Sci. Rep. 9, 14150, 10.1038/s41598-019-50700-4.
Oh, S.Y., Cho, K.A., Kang, J.L., et al., 2014. Comparison of experimental mouse models of inflammatory bowel disease. Int. J. Mol. Med. 33, 333–340. https://doi.org/10.3892/ijmm.2013.1569.
Pinato, D.J., Howlett, S., Ottaviani, D., et al., 2019. Association of prior antibiotic treatment with survival and response to immune checkpoint inhibitor therapy in patients with cancer. JAMa Oncol. 5, 1774–1778. https://doi.org/10.1001/jamaoncol.2019.2785.
Prescott, J.F., 1991. *Rhodococcus equi*: an animal and human pathogen. Clin. Microbiol. Rev. 4, 20–34. https://doi.org/10.1128/CMR.4.1.20.
Qiao, K., Han, J., Zhang, H., et al., 2023. Intratumor Mycoplasma promotes the initiation and progression of hepatocellular carcinoma. Cell Rep. 42, 113563. https://doi.org/10.1016/j.celrep.2023.113563.
Ramanan, D., Pratama, A., Zhu, Y., et al., 2023. Regulatory T cells in the face of the intestinal microbiota. Nat. Rev. Immunol. 23, 749–762. https://doi.org/10.1038/s41577-023-00890-w.
Rao, Y., Kuang, Z., Li, C., et al., 2021. Gut *Akkermansia muciniphila* ameliorates metabolic dysfunction-associated fatty liver disease by regulating the metabolism of L-aspartate via gut-liver axis. Gut. Microbes 13, 1–19. https://doi.org/10.1080/19490976.2021.1927633.
Sakaguchi, I., Ikeda, N., Nakayama, M., et al., 2000. Trehalose 6,6′-dimycolate (Cord factor) enhances neovascularization through vascular endothelial growth factor production by neutrophils and macrophages. Infect. Immun. 68, 2043–2052. https://doi.org/10.1128/iai.68.4.2043-2052.2000.
Sibai, M., Altuntaş, E., Yıldırım, B., et al., 2020. Microbiome and longevity: high abundance of longevity-linked muribaculaceae in the gut of the long-living rodent spalax leucodon. OMICS-J. Integr. Biol. 24, 592–601. https://doi.org/10.1089/omi.2020.0116.
Singal, A.G., Lampertico, P., Nahon, P., 2020. Epidemiology and surveillance for hepatocellular carcinoma: new trends. J. Hepatol. 72, 250–261. https://doi.org/10.1016/j.jhep.2019.08.025.
Su, Y., Wang, H.K., Gan, X.P., et al., 2021. Alterations of gut microbiota in gestational diabetes patients during the second trimester of pregnancy in the Shanghai Han population. J. Transl. Med. 19, 366. https://doi.org/10.1186/s12967-021-03040-9.
Sun, L., Ke, X., Guan, A., et al., 2023a. Intratumoural microbiome can predict the prognosis of hepatocellular carcinoma after surgery. Clin. Transl. Med. 13, e1331. https://doi.org/10.1002/ctm2.1331.
Sun, P., Li, Z., Zhang, B., 2023b. Characterization of disease-associated microbiota in hepatocellular carcinoma. J. Cancer Res. Ther. 19, 881–891. https://doi.org/10.4103/jcrt.jcrt_139_22.
Sun, Y., Wang, F., Liu, Y., et al., 2022. Microbiome-metabolome responses of Fuzhuan brick tea crude polysaccharides with immune-protective benefit in cyclophosphamide-induced immunosuppressive mice. Food Res. Int. 157, 111370. https://doi.org/10.1016/j.foodres.2022.111370.
Uehara, T., Pogribny, I.P., Rusyn, I., 2014. The DEN and CCl4 -induced mouse model of fibrosis and inflammation-associated hepatocellular carcinoma. Curr. Protoc. Pharmacol. 66. https://doi.org/10.1002/0471141755.ph1430s66, 14.30.1-14.30.10.
Vail, K.J., da Silveira, B.P., Bell, S.L., et al., 2021. The opportunistic intracellular bacterial pathogen *Rhodococcus equi* elicits type I interferon by engaging cytosolic DNA sensing in macrophages. PLoS. Pathog. 17, e1009888. https://doi.org/10.1371/journal.ppat.1009888.
Wang, J., Lu, R., Fu, X., et al., 2018. Novel regulatory roles of Wnt1 in infection-associated colorectal cancer. Neoplasia 20, 499–509. https://doi.org/10.1016/j.neo.2018.03.001.
Wang, M., Zhang, S., Zhong, R., et al., 2021. Olive fruit extracts supplement improve antioxidant capacity via altering colonic microbiota composition in mice. Front. Nutr. 8, 645099. https://doi.org/10.3389/fnut.2021.645099.
Wang, W., Lin, L., Du, Y., et al., 2019. Assessing the viability of transplanted gut microbiota by sequential tagging with D-amino acid-based metabolic probes. Nat. Commun. 10, 1317. https://doi.org/10.1038/s41467-019-09267-x.
Wang, W., Liu, Z., Yue, W., et al., 2022. Mucosa-colonizing microbiota correlate with host autophagy signaling in patients with inflammatory bowel disease. Front. Microbiol. 13, 875238. https://doi.org/10.3389/fmicb.2022.875238.
Wang, X., Fang, Y., Liang, W., et al., 2025. Gut-liver translocation of pathogen Klebsiella pneumoniae promotes hepatocellular carcinoma in mice. Nat. Microbiol. 10, 169–184. https://doi.org/10.1038/s41564-024-01890-9.
Wiegand, I., Hilpert, K., Hancock, R.E., 2008. Agar and broth dilution methods to determine the minimal inhibitory concentration (MIC) of antimicrobial substances. Nat. Protoc. 3, 163–175. https://doi.org/10.1038/nprot.2007.521.
Xiang, H., Liu, Z., Xiang, H., et al., 2022. Dynamics of the gut-liver axis in rats with varying fibrosis severity. Int. J. Biol. Sci. 18, 3390–3404. https://doi.org/10.7150/ijbs.69833.
Xing, T., Benderman, L.J., Sabu, S., et al., 2020. Tight junction protein claudin-7 is essential for intestinal epithelial stem cell self-renewal and differentiation. Cell Mol. Gastroenterol. Hepatol. 9, 641–659. https://doi.org/10.1016/j.jcmgh.2019.12.005.
Yamada, S., Takashina, Y., Watanabe, M., et al., 2018. Bile acid metabolism regulated by the gut microbiota promotes non-alcoholic steatohepatitis-associated hepatocellular carcinoma in mice. Oncotarget. 9, 9925–9939. https://doi.org/10.18632/oncotarget.24066.
Yan, S., Chen, J., Zhu, L., et al., 2022. Oryzanol alleviates high fat and cholesterol diet-induced hypercholesterolemia associated with the modulation of the gut microbiota in hamsters. Food Funct. 13, 4486–4501. https://doi.org/10.1039/d1fo03464b.
Yoshimoto, S., Loo, T.M., Atarashi, K., et al., 2013. Obesity-induced gut microbial metabolite promotes liver cancer through senescence secretome. Nature 499, 97–101. https://doi.org/10.1038/nature12347.
Yu, J., Zhu, P., Shi, L., et al., 2024. Bifidobacterium longum promotes postoperative liver function recovery in patients with hepatocellular carcinoma. Cell Host. Microbe 32, 131–144. https://doi.org/10.1016/j.chom.2023.11.011.
Yu, Y., Liu, B., Liu, X., et al., 2022. Mesenteric lymph system constitutes the second route in gut-liver axis and transports metabolism-modulating gut microbial metabolites. J. Genet. Genom. 49, 612–613. https://doi.org/10.1016/j.jgg.2022.03.012.
Zhao, F., Chen, Y., Gao, J., et al., 2021. Characterization of vaginal microbiota in women with recurrent spontaneous abortion that can be modified by drug treatment. Front. Cell Infect. Microbiol. 11, 680643. https://doi.org/10.3389/fcimb.2021.680643.
Zhao, Z., Chen, L., Zhao, Y., et al., 2020. *Lactobacillus plantarum NA136* ameliorates nonalcoholic fatty liver disease by modulating gut microbiota, improving intestinal barrier integrity, and attenuating inflammation. Appl. Microbiol. Biotechnol. 104, 5273–5282. https://doi.org/10.1007/s00253-020-10633-9.